Chapter 15

The Role and Form of Modelling in Space Weather

Konstantinos Papadopoulos
Departments of Physics and Astronomy, University of Maryland
College Park, MD 20782, USA

Abstract A critical element of the space weather research and forecasting is the development and use of models. Models vary in form, content, context and sophistication. On one extreme are the contemporary forecasting models, based on heuristic algorithms, statistical relationships, and human estimates currently in use in space weather forecasting and system engineering design. On the other extreme are physics based, dynamic, quantitative models, critical in understanding the fundamental chain of physical processes that affect the state of the sun, magnetosphere, ionosphere, and atmosphere, and their couplings and feedback; the elements that constitute and control the space weather. It is clear that physics based models, such as MHD, hybrid and particle codes, have played and will continue to play a critical role in answering research questions. The important issue at hand is to what extent physics based models can, by themselves or in combination with statistical or non-linear dynamics models, become real time forecasting tools. This tutorial will first review the types of models currently in use in space weather, with emphasis on their strengths and limitations. This will be followed by the presentation of several magnetospheric storms and substorms recorded by ground and space based instruments and compared with data driven simulations using the Lyon-Fedder-Mobarry model. These examples will be used as aides in the assessment of the utility and limitations of physics based models in space weather and in addressing issues such as validation, testing and implementation of such models as research and forecasting tools.

Keywords Space weather, modelling, MHD, substorm, magnetic storm, LFM model, magnetosphere, ionosphere, magnetosphere-ionosphere coupling.

I.A. Daglis (ed.), Space Storms and Space Weather Hazards, 389–400.

1. INTRODUCTION

The ultimate objective of space weather research is the development of quantitative forecasting models. There are two generic classes of forecasting models, system models and first principles models. System models – empirical, statistical or non-linear dynamics – are the only ones currently used in forecasting. Their main advantage is their minimal algorithmic complexity, which permits real time implementation. Their biggest problem is reliability, a generic issue to all empirical modelling. First principle models - models that rely on well founded closed sets of mathematical equations derived from well-founded physical principles - have always been important in addressing research questions. Their biggest problem is the enormous computer power required to achieve the required spatial and temporal resolution.

The critical current question in modelling is the feasibility and extent to which first principles models, by them selves or in some combination with system models, can be used as real time forecasting tools. As is obvious from previous talks in the school and the workshop, this is an actively debated issue. This issue will not be explicitly addressed in this review, because I believe that the answer depends on the specific requirements and reliability. Instead, I will present the background information that, in conjunction of the other workshop presentations, will allow you to reach your own conclusions. Time constraints force me to be selective on the issues and examples I will present, as well as parochial since for my personal convenience and availability of graphics I selected mostly examples from the University of Maryland group.

2. ELEMENTS OF SPACE WEATHER

The critical elements of space weather are shown in Figure 1.

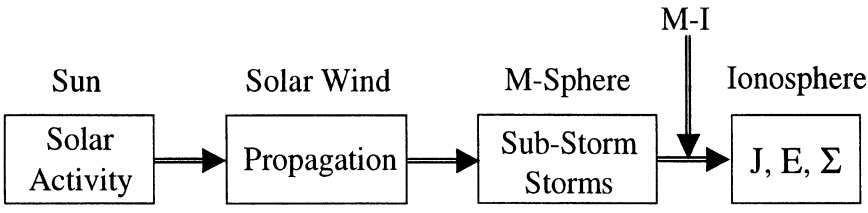

Figure 1. Critical elements of Space Weather

The cause of space weather is the active Sun that generates disturbances in the form of Solar Flares and Coronal Mass Ejections (CME). The disturbances propagate towards the earth where they interact with the earth's magnetosphere and ionosphere. The effects of space weather are manifested mostly in the radiation belts, in the form of enhanced particle fluxes, the ionosphere, in the form of strong current systems and perturbations in the electron density, and on the ground in the form of strong and dynamic electromagnetic fields. All of the components of space weather shown in Figure 1 have intellectually challenging research and forecasting questions. Previous talks at the conference addressed the first two components. In this talk I will emphasize the last two components. The strongly non-linear response of the magnetosphere to the solar wind input and its coupling and feedback with the ionosphere are perhaps the most critical elements determining the geo-effectiveness of the solar disturbance.

3. GLOBAL GEO-SPACE MODELS – THE LFM MODEL

The development of space weather models can be guided to a great extent by the modelling effort of the International Solar Terrestrial Program (ISTP). The objective of ISTP was the quantitative understanding of the flow of energy, mass and momentum through geo-space. The Space and Plasma Physics (SPP) group at the University of Maryland was tasked with the development of the first three-dimensional (3D), global, dynamic "cause and effect" models that utilize dynamic input from the ISTP satellites. A methodology was developed that:

- Was compatible with computer resources and state of the art physics.
- Utilized as best as possible the space and ground based ISTP measurements; first as input to the code and then as test-bed of the results.

This led to the development of a 3D MHD code interactively coupled to a 2D electrostatic, height-integrated ionospheric model. The model, known as the LFM (Lyon-Fedder-Mobarry) model from the initial of its authors, is driven by dynamic input upstream provided by satellites. Subsidiary models received input from LFM to address local problems. Extensive diagnostic and visualization tools were developed to complement the effort.

The magnetospheric part of the LFM model was based on the solution of the 3D ideal MHD equations in a conservative form given below:

$$\frac{\partial \rho}{\partial t} + \nabla \cdot (\rho \mathbf{u}) = 0$$

$$\frac{\partial}{\partial t}(\rho \mathbf{u}) + \nabla \cdot \left[\rho \mathbf{u}\mathbf{u} + \left(p + \frac{B^2}{8\pi} \right) \mathbf{I} - \frac{\mathbf{B}\mathbf{B}}{4\pi} \right] = 0$$

$$\frac{\partial \mathbf{B}}{\partial t} + \nabla \cdot (\mathbf{u}\mathbf{B} - \mathbf{B}\mathbf{u}) = 0$$

$$\frac{\partial}{\partial t}(\rho E) + \nabla \cdot \left[\mathbf{u} \left(\rho E + p + \frac{B^2}{8\pi} \right) - \mathbf{B}(\mathbf{u} \cdot \mathbf{B}) \right] = 0$$

with

$$\rho E = \frac{1}{2} \rho u^2 + \frac{p}{\gamma + 1} + \frac{B^2}{8\pi}$$

$$\nabla \cdot \mathbf{B} = 0$$

These equations are discretized and solved on a cylindrical staggered mesh, typically 60 R_E in radius and 330 R_E long, containing the solar wind and the magnetosphere. A spider web type of computational grid places maximal resolution on critical locations. The code uses diffuse solar wind matching conditions along the outer edges of the computational domain. This allows use of time dependent solar wind parameters as input conditions. A simple supersonic outflow condition is used at the far boundary. The inner boundary condition is located on a geocentric sphere of radius 2-3 R_E, where the magnetospheric solution is matched to an ionospheric model. The ionospheric model solves the 2D height integrated electrostatic potential equation driven by the field-aligned currents within the magnetosphere,

$$\nabla \cdot \Sigma \cdot \nabla \Phi = \mathbf{J} \cdot \mathbf{B}$$

where Φ is the ionospheric potential and Σ the ionospheric conduction tensor. The $\mathbf{J} \cdot \mathbf{B}$ term represents the Magnetosphere-Ionosphere (MI) coupling. Solar UV and auroral conductance models were used for Σ. To include dipole rotation, the simulations are usually performed in SM coordinates. Details of the code and of the numerical algorithms can be found in Wiltberger (1998). Before implementation the code was

successfully tested against several standard numerical problems. The code initialization is shown graphically in Visualization #1. We start with the earth's dipole magnetic field and allow the solar wind to flow and form its steady state configuration.

The LFM diagnostics and subsidiary models were tailored to the determination of the solar terrestrial energy chain shown in Figure 2.

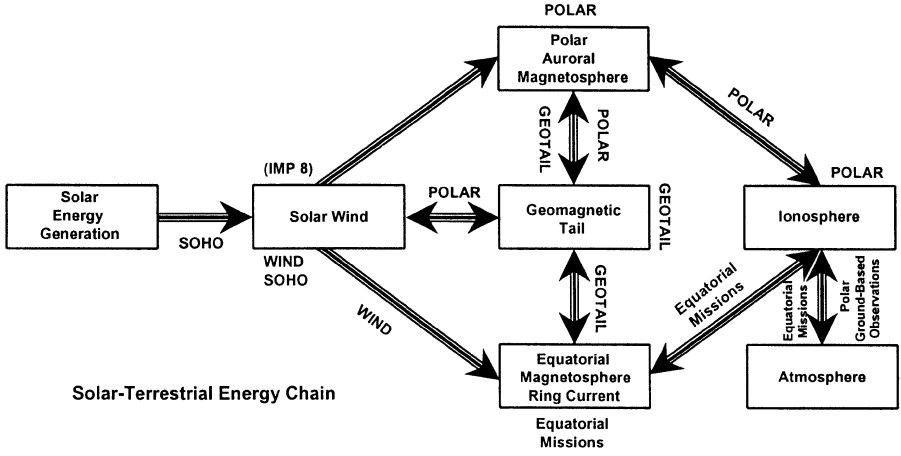

Figure 2. The solar-terrestrial energy chain: the sun's energy flows from the interior through the photosphere, corona, and interplanetary medium to the vicinity of the earth where it interacts with the geomagnetic field and atmosphere.

The main LFM code was complemented with subsidiary models that describe the radiation belts, and extensive output modules that allow comparison with measurements and assessment of metrics and extensive visualization tools. The structure of the complete model is shown in Fig. 3.

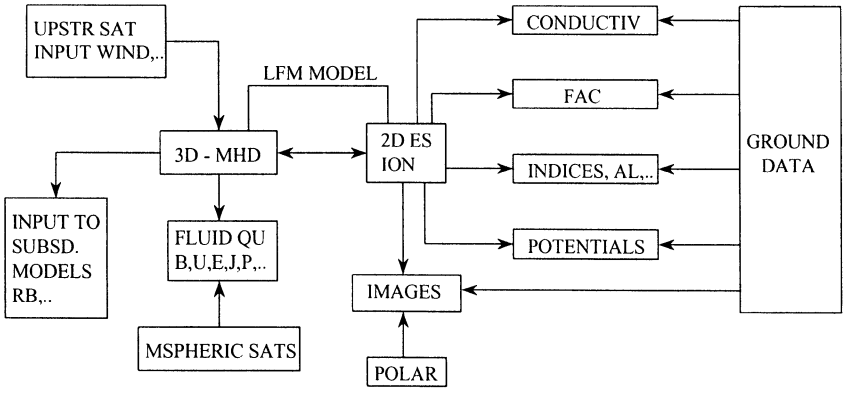

Figure 3. LFM model including subsidiary codes and diagnostic output

4. CASE STUDIES

The first serious case study using real data was the substorm that occurred on March 9, 1995. This event occurred before the launch of the Polar satellite so the main comparison with data was through the ground magnetometer response. What was remarkable in this event was the timing accuracy and similarity between the CANOPUS magnetometer measurements and the simulations.

The event started with a long, longer than 8 hours, northward IMF, which allowed the magnetosphere to approach a "ground state" configuration. At approximately 0330 UT a rotational discontinuity reached the earth, imposing a southward IMF on the magnetospheric boundary. Shortly afterward ground magnetometers recorded signatures consistent with growth phase.

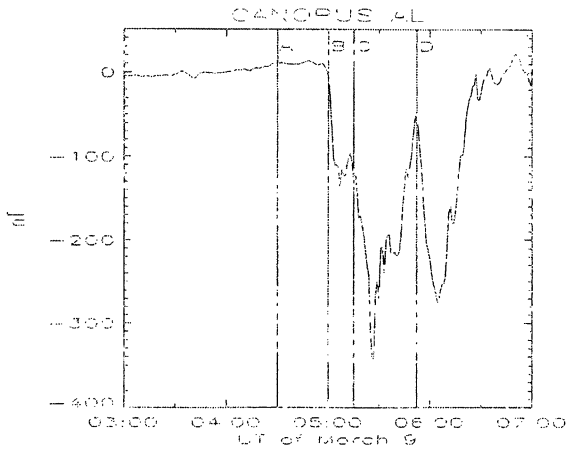

Figure 4a. CL index using CANOPUS the magnetometer array (March 9, 1995)

Figure 4a shows the CL index constructed from the CANOPUS array of magnetometers. The index shows a weak eastward electrojet associated with the substorm phase (A) at 0430 UT, onset at 0500 (B), intensification at 0520 (C), recovery from 0530 to 0552, and a second onset (D). The same features and timing are apparent in the simulation data (Figure 4b).

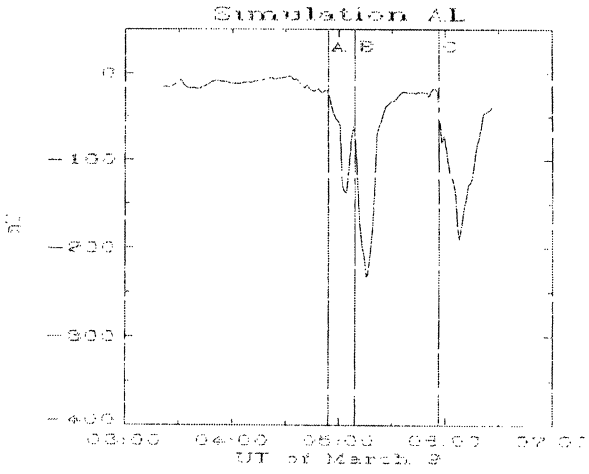

Figure 4b. CL constructed from the LFM simulations

We present next a series of visualizations (Visualizations #2—6 in the accompanying CD-ROM) from the output of the LFM simulations pertaining to this case. It is important that the visualizations be viewed in conjunction with the timing of the phases A, B, and C, seen in Figures 4 and described above. For a more detailed description of this case we refer the reader to Lopez et al. (1998) and Papadopoulos et al. (1999). Visualization #2 shows simulations describing the dynamic evolution of the surface of the last closed magnetic field lines shown as a translucent surface. On the left of each frame is the clock angle of the IMF and the arrow is proportional to the log of the ram pressure. The density is colour coded, while the arrows are flow vectors. In visualization #3 the initial state occurs at 0300 UT and is consistent with northward IMF configuration. Substorm signatures appear at 0456 and 0511. Notice in particular the appearance of hot plasma (orange surface) in the vicinity of 10 R_E. This substorm behaviour is consistent with the CL behaviour shown above and satellite measurements. The various phases of the substorm are also in evidence in the Visualization #3. This Visualization is similar to Visualization #2 but the colour plots represent the value of the electric field instead of the density. It is important to note the low value of the electric field early on. At 0456 a reconnection region forms near 30 R_E, while an enhanced electric field appears in the inner tail region (<10 R_E). This field is far from the reconnection region that is far down the tail. The Visualization shows that after the electric field impulse reached the centre of the plasma sheet it launched a tail-ward propagating signal. When the signal reaches the reconnection region enhances its rate significantly as seen from the associated flows: close to 10 R_E at substorm onset. Visualization #4 shows in a dramatic fashion the reconfiguration of the tail.

The final two Visualizations #5 and #6 show the evolution of the field aligned current and plasma flows in the equatorial plane. Notice the formation of current filaments and the current diversion towards the aurora.

A real test of the model and its capabilities occurred in January 1997. For the first time ever the ISTP satellites tracked a solar eruption, from the CME expelled from the Sun, through interplanetary space, until it encountered the earths magnetosphere, causing violent disturbances and spectacular auroral displays. The explosion started on the Sun January 6, 1997, and the magnetic cloud hit the earth on January 10. Following its arrival there were many communications disruptions and the loss of a TELSTAR satellite. The simulation of the event was a grand challenge problem and a computational coup-de-force. The simulation covered 42 hours of real time, required 160 C90 CPU hours, and produced over 6 GB of data. Details of the case are discussed in Goodrich et al. (1998) and shown graphically in Visualization #7. The format is similar to Visualization #2, except that in the lower right side the UV emission in the northern hemisphere is shown as computed by the code. There was good agreement with Polar observations. The period can be divided into three case segments. Between 0100-0300 UT the magnetosphere was in a closed tadpole like configuration. The first significant activity started at 0300 UT with a modest substorm onset at 0315 UT. The magnetosphere expanded to a more relaxed state between 0340 and 0410 UT. The arrival of the magnetic cloud marked the beginning of the next period, 0500-1500 UT, characterized by a large reduction in density and temperature. The decrease in ram pressure caused bow shock motion outwards. Strong activity occurs till 0600 UT. An approximate equilibrium occurs between 0600-0700 UT. Sudden increase in ram pressure at 0700 UT leads to increased emission. Ionospheric activity with significant intensifications correlates well with density pulses at 0730, and 0840. The last period occurred between 1500 January 10 and 0300 January 11 and was characterized by steady northward IMF. However, beginning at 2200 UT the density increased gradually reaching values between 100 and 180 #/cm^3. The enormous increase in pressure, as seen clearly in the simulations, resulted in moving the dayside magnetopause well within the geo-synchronous orbit. This period is not included in the CD-ROM, but it can be obtained at the Space Plasma Physics group's website: www.spp.astro.umd.edu/Research/Mhd/mhd.htm. Notice that unlike earlier pulses this more massive pulse resulted in minimal ionospheric activity due to the northward IMF orientation.

5. CODE VALIDATION – IMPROVEMENTS

In testing the code against ground-based observations, we found that while there was relatively good agreement with the CANOPUS magnetometer chain, the results of the code were totally inconsistent with riometer data. This is evident from Figure 5a, which shows the VHF (38 MHz) absorption measured by the riometers at three different locations during 10 January 1997 (solid trace) along with the model results (dashed trace). The riometers were located in Sondersrom, Ingaluit and Gakona, Alaska. This led to further research to identify the causes of the discrepancy and improve the appropriate part of the code. In examining the times of the major discrepancies we realized that they coincided with the times that the electrojet current was very large. This led us to hypothesize that instabilities connected with the electrojet might result in turbulent electron heating caused by electrojet instabilities. The non-linear theory of the modified two-stream instability, also known as the Farley-Buneman instability, was developed by Ossakow et al (1974). Later on Schlegel and St-Maurice (1981) using radar observations confirmed that the electron temperature rises significantly in the polar electrojet during substorms. In view of this we developed a model that describes the temporally and spatially averaged electron temperature, based on non-linear physics considerations and comparison with available radar observations of the electron heating. The model gives good agreement with the observations. When anomalous heating is taken into consideration the agreement between the computed VHF absorption and observations improves considerably. This is shown in Figure 5b, where the VHF absorption measured by the riometers at the above three locations is shown by solid trace while, the model results are shown by dashed trace.

We expect that inclusion of anomalous collision frequency in the ionospheric conductance could improve the MHD model by providing feedback between the model ionosphere, serving as a dynamic boundary condition, and the 3-D global magnetospheric simulations.

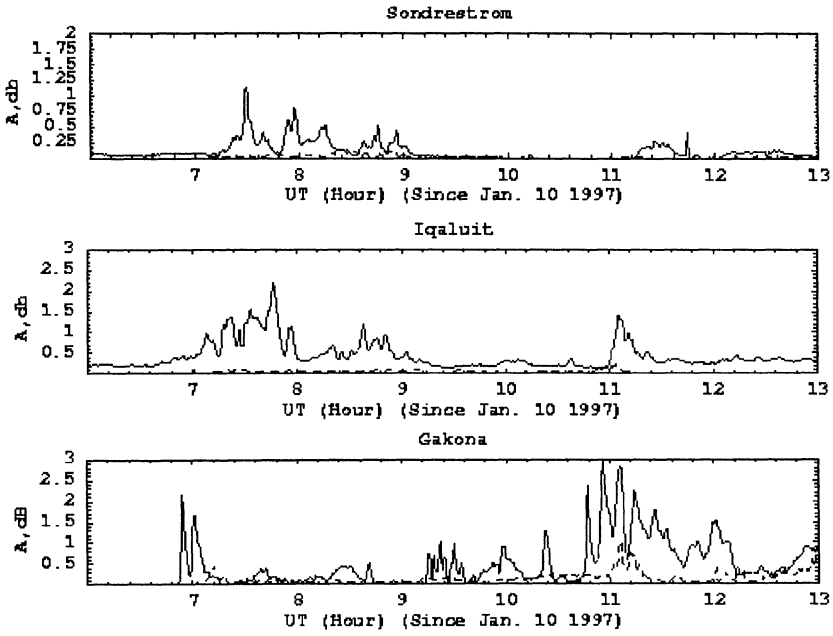

Figure 5a. Comparison of the code results with data, without turbulent heating

6. CONCLUDING REMARKS

The purpose of this tutorial was to review the progress in first-principles magnetospheric modelling during the last 20 years, using case studies. There is no question that enormous progress has been achieved from the cartoons and the steady state models of the seventies to today's data driven dynamic models. We have learned that geo-space is dynamic, and static equilibrium seldom applies. Average and statistical models are good for classification but not for forecasting. Are then first principles models ready for implementation in space weather forecasting? I hope I gave you enough information to make up your own mind. My answer is a qualified may be. It clearly depends on the objective and the required reliability. A major issue is reliability and lack of automation. It reminds me of a new chemical analysis tool, measuring blood count for example, that requires several PhD scientists to analyse and interpret. While the overall approach is promising we have not yet analysed sufficient cases to develop the proper sixth sense. Let us not forget that the art of modelling complex systems is simplification.

Getting rid of all the little details while keeping the essence. We are still keeping too many details and under-resolving important areas. We can reach this stage only by using our current tools to examine as many cases as possible.

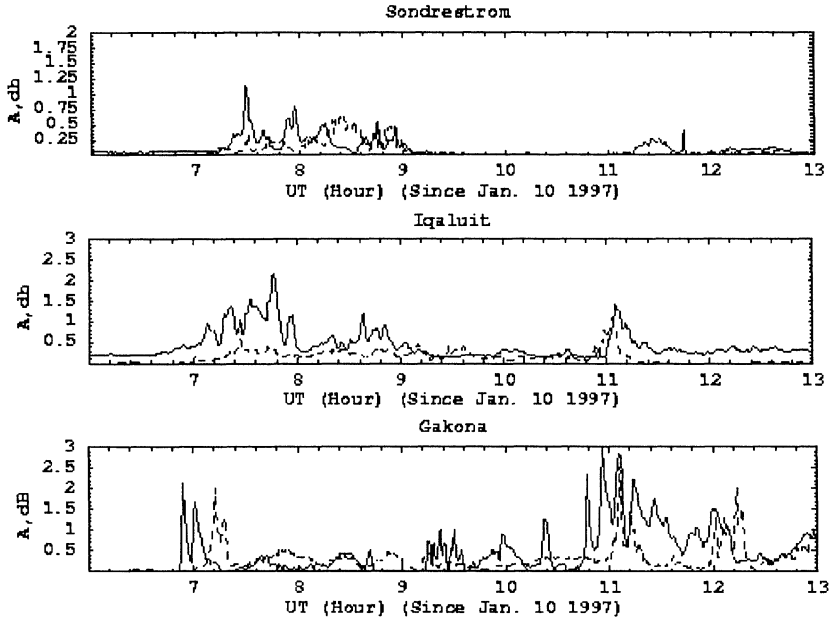

Figure 5b. Comparison of the code results with data, *with* turbulent heating

7. ACKNOWLEDGEMENTS

While I presented the tutorial, the credit should go to the Space and Plasma Physics group at the University of Maryland that formed the core of the ISTP modelling work. I would like to thank in particular Drs C. Goodrich, M. Wiltberger, J. Lyon (Dartmouth College), X. Shao, G. Milikh, P. Guzdar, R. Lopez and S. Sharma for providing with the material of the presentation. They are the true authors of the paper.

8. REFERENCES

Goodrich, C. C., W. Wiltberger, R. E. Lopez and K. Papadopoulos, An Overview of the Impact of the January 10-11, 1997 Magnetic Cloud on the Magnetosphere via Global MHD Simulations, *Geophys. Res. Lett.*, **25**, 2537-2540, 1998.

Lopez, R., C. Goodrich, M. Wiltberger, K. Papadopoulos and J. L. Lyon, Substorm Onset and Evolution: Coupling Between Tail Regions in MHD Simulations, *Physics of Space Plasmas*, 1998.

Ossakow, S., K. Papadopoulos, J. Orens, and T. Coffey, Parallel Propagation Effects on the Type I Electrojet Instability, *J. Geophys. Res.*, *80*, 141, 1975.

Papadopoulos, K., C. C. Goodrich, M. Wiltberger, R. E. Lopez and J. G. Lyon, The Physics of Substorms as Revealed by the ISTP, *Physics and Chemistry of the Earth,* **24**, 1-3, 189-202, 1999.

Schlegel, K. and J.P. St-Maurice, Anomalous Heating of the Polar E region by Unstable Plasma Waves -1. Observations, *J. Geophys. Res.*, **86A**, 1447-1452, 1981.

Wiltberger, M. S., Global Magnetohydrodynamic Simulations of Magnetospheric Substorms, Ph. D. Dissertation, University of Maryland, College Park, 1998.